J Neurophysiol
88: 740–750, 2002; 10.1152/jn.00635.2001.

Synaptic Inhibition of Pyramidal Cells Evoked by Different Interneuronal Subtypes in Layer V of Rat Visual Cortex

ZIXIU XIANG, JOHN R. HUGUENARD, AND DAVID A. PRINCE
Stanford University School of Medicine, Department of Neurology and Neurological Sciences, Stanford, California 94305

Received 1 August 2001; accepted in final form 12 April 2002

Xiang, Zixiu, John R. Huguenard, and David A. Prince. Synaptic inhibition of pyramidal cells evoked by different interneuronal subtypes in layer V of rat visual cortex. *J Neurophysiol* 88: 740–750, 2002; 10.1152/jn.00635.2001. Properties of $GABA_A$ receptor-mediated unitary inhibitory postsynaptic currents (uIPSCs) in pyramidal (P) cells, evoked by fast spiking (FS) and low-threshold spike (LTS) subtypes of interneurons in layer V of rat visual cortex slices were examined using dual whole cell recordings. uIPSCs evoked by FS cells were larger and faster rising than those evoked by LTS cells, consistent with the known primary projections of FS and LTS cell axons to perisomatic and distal dendritic areas of layer V pyramidal cells, respectively, and the resulting electrotonic attenuation for LTS-P synaptic events. Unexpectedly, the decay time constants for LTS-P and FS-P uIPSCs were not significantly different. Modeling results were consistent with differences in the underlying $GABA_A$ receptor–mediated conductance at LTS-P and FS-P synapses. Paired-pulse depression (PPD), present at both synapses, was associated with an increase in failure rate and a decrease in coefficient of variation, indicating that presynaptic mechanisms were involved. Furthermore, the second and first uIPSC amplitudes during PPD were not inversely correlated, suggesting that PPD at both synapses is independent of previous release and might not result from depletion of the releasable pool of synaptic vesicles. Short, 20-Hz trains of action potentials in presynaptic interneurons evoked trains of uIPSCs with exponentially decreasing amplitudes at both FS-P and LTS-P synapses. FS-P uIPSC amplitudes declined more slowly than those of LTS-P uIPSCs. Thus FS and LTS cells, with their differences in firing properties, synaptic connectivity with layer V P cells, and short-term synaptic dynamics, might play distinct roles in regulating the input-output relationship of the P cells.

INTRODUCTION

GABAergic inhibitory interneurons play critical roles in information processing, plasticity, and synchronous activity in the neocortex (Somogyi et al. 1998). They constitute between 10 and 20% of the total neuronal population in the cortex and are known to be heterogeneous in morphology, spike-firing properties, and immunocytochemical reactivity (Gupta et al. 2000; Hendry et al. 1984, 1989; Houser et al. 1983; Jones and Hendry 1984; Kawaguchi et al. 1995; Somogyi et al. 1984; Thomson et al. 1996). In layer V of the neocortex, there are several subtypes of electrophysiologically distinct interneurons, including low threshold spike (LTS) and fast spiking (FS) cells. These two subtypes also have different immunoreactivities for calcium binding proteins; FS cells contain pavalbumin and LTS cells mainly contain calbindin (Kawaguchi and Kubota 1993). In addition, the two interneuronal types have distinct intracortical axonal projection patterns. The axons of FS interneurons in layer V tend to be distributed mostly horizontally, whereas LTS cells have more vertical axonal arborizations (Jones and Hendry 1984; Kawaguchi and Kubota 1993), indicating that they might make synaptic connections on different soma-dendritic domains of the principal cells. Indeed, neocortical FS cells were found to make synapses primarily onto somatic and proximal dendritic areas of the pyramidal (P) cells, including those in layer V (Tamas et al. 1997; Thomson et al. 1996). The axon terminals of LTS interneurons appeared to innervate more distal regions of P cell dendritic trees, rather than perisomatic areas (DeFelipe et al. 1989; Deuchars and Thomson 1995; Thomson et al. 1996). Furthermore, the excitability of these two types of interneurons could be differentially modulated by the neurotransmitter acetylcholine (Xiang et al. 1998a).

To investigate the different roles of FS cells and LTS cells in regulating the functions of pyramidal neurons, we compared the kinetics and short-term plasticity of unitary inhibitory postsynaptic currents (uIPSCs) at FS-P and LTS-P synapses in layer V of the rat visual cortex, using dual whole cell recordings from interneuronal P cell pairs. We found that uIPSCs in P cells evoked by action potentials (APs) in FS cells are significantly larger in amplitude and faster in rise time than those following APs in LTS interneurons. Both synapses showed paired-pulse depression (PPD). Short-term synaptic dynamics are different between these two synapses with uIPSC amplitude decaying faster at LTS-P synapses than at FS-P synapses. The results indicate that these two types of interneurons with distinct firing patterns and axonal arborizations play different functional roles in controlling the input-output relation of pyramidal cells.

METHODS

Slice preparation

Neocortical slices were prepared as previously described in detail (Xiang et al. 1998b). In brief, coronal visual cortical slices (350 μm) were cut from brains of young Sprague-Dawley rats (P12–P15) using a vibratome (Series 1000; Technical Products International, St. Louis,

Present address and address for reprint requests: Z. Xiang, Dept. of Anatomy and Neurobiology, University of Tennessee, 875 Monroe Ave., Memphis, TN 38163

The costs of publication of this article were defrayed in part by the payment of page charges. The article must therefore be hereby marked "*advertisement*" in accordance with 18 U.S.C. Section 1734 solely to indicate this fact.

MO). Ice-cold oxygenated (95% O_2-5% CO_2) "cutting solution" contained (in mM) 230 sucrose, 2.5 KCl, 0.5 $CaCl_2$, 10 $MgSO_4$, 1.25 NaH_2PO_4, 26 $NaHCO_3$, and 10 D-glucose (pH 7.4). Slices were incubated in oxygenated artificial cerebrospinal fluid (ACSF) at 32°C for at least 1 h. The ACSF contained (in mM) 126 NaCl, 3 KCl, 2 $CaCl_2$, 2 $MgSO_4$, 1.25 NaH_2PO_4, 26 $NaHCO_3$, and 10 D-glucose. Slices were transferred, one at a time, to the recording chamber where they were superfused with ACSF and maintained at 32–33°C.

Electrophysiological recordings

Simultaneous dual whole cell patch recordings were made from visually identified interneurons and P cells in layer V under infrared video microscopy with Nomarski optics. An Axoclamp 2B (Axon Instruments, Foster City, CA) was used for current-clamp recordings from interneurons, and an EPC-7 patch amplifier (List Electronics, Greenville, NY) was used for voltage-clamp recordings from P cells. Patch pipettes were prepared from borosilicate glass (Warner Instrument, Hamden, CT) using a Flaming-Brown micropipette puller (Model P-80/PC; Sutter Instruments, Novato, CA). They had resistances of 3–4 MΩ when filled with the pipette solution containing (in mM) 65 KCl, 65 potassium gluconate, 1 $MgCl_2$, 1 $CaCl_2$, 10 HEPES, 10 EGTA, 3 ATP, and 0.2–0.4 GTP. Biocytin (0.2–0.3% wt/vol) was also included in the pipette solution. The pH was adjusted to 7.3 with KOH. The mean value of the series resistance for the postsynaptic cells included in the analysis was 8.8 ± 0.3 MΩ ($n = 22$). Recordings with change in series resistance of >10% were rejected. The calculated chloride equilibrium potential (E_{Cl}) was −15 mV, based on the Nernst equation, with activity coefficients for extracellular Cl^- of 0.76 and intracellular Cl^- of 0.80, and taking into account the permeability of gluconate through Cl^- channels (Barker and Harrison 1988). uIPSCs were recorded from P cells at a holding potential (V_h) of −80 mV, and evoked by interneuron APs elicited by brief depolarizing current pulses (5–10 ms, 200–400 pA) every 8 s. Under these recording conditions, IPSCs were inward currents.

In experiments in which sucrose-induced miniature IPSCs (mIPSCs) were examined, 1 M sucrose was applied by pressure pulses (20–30 kPa, 100–250 ms) via a patch pipette (2–3 μm in tip diameter) placed approximately 50 μm away from the recorded P cell soma. The pressure pulses were generated by a customized device consisting of an air pressure regulator, a compressed air cylinder, and a solenoid operated miniature valve controlled by a pulse generator (WPI). Ionotropic glutamate receptor antagonists, 6,7-dinitroquinoxoline-2,3-dione (DNQX, 20 μM), 2-amino-5-phosphonopentanoic acid (APV, 50 μM), and voltage-gated sodium channel blocker, tetrodotoxin (TTX, 1 μM) were included in the perfusate. In a preliminary experiment in which Sr^{2+}-induced asynchronous IPSCs were assessed (Morishita and Alger 1997; Ohno-Shosaku et al. 1994), we substituted 2 mM $SrCl_2$ for 2 mM $CaCl_2$ in the ACSF and found that the amplitude of uIPSCs decreased, but delayed asynchronous release was not apparent. However, in subsequent experiments, inclusion of 4 mM $SrCl_2$ in the regular ACSF along with $CaCl_2$ (2 mM) was sufficient to cause an increase in the frequency of delayed asynchronous currents and a decrease in the amplitude of uIPSCs.

Data analysis

A computer equipped with PCLAMP (Axon Instruments) and Strathclyde Electrophysiology Software (J. Dempster) was used to generate the pulses, digitize, and record data on-line. Data were also digitized (44 kHz) by a Neurocorder DR-484 (Neuro Data Instruments) and stored on videotape for off-line analysis. The following software packages were used for data analysis, SCAN (J. Dempster), Origin (Microcal), Clampex (Axon Instrument), and the locally written programs, Metatape and Detector (Ulrich and Huguenard 1996). The uIPSC amplitude was measured as the difference between the postsynaptic current during a 1-ms time window at its peak and the baseline current taken from a 2-ms time window close to the onset (Fig. 4*A3*). The noise amplitude measurements were taken from a 1-ms time window 3 ms prior to baseline for the first IPSCs. Interneurons were classified as LTS cells and FS cells based on their spike firing properties under current-clamp conditions (Xiang et al. 1998a). The 10–90% rise time, decay time constant (τ_D), and onset latency of uIPSCs were measured from average traces, which were obtained from multiple IPSCs, each aligned to the peak of the presynaptic AP. Onset latency was defined as time interval between the peak of the presynaptic action potential and the time point at which the evoked IPSC rose to 10% of its peak value.

The sucrose-induced mIPSCs were automatically detected by the customized program Detector, using the derivative of the digitally filtered current traces (cutoff, 800 Hz) as the trigger (Ulrich and Huguenard 1996). Detected events were classified into three types: IPSCs consisting of a single peak with smooth rise and decay time courses (type I), compound events that arose from a flat baseline with one or more other events riding on their decay phase (type II), and IPSCs that occurred on the falling phase of a preceding events (type III). Only type I and II events were used to construct amplitude histograms. The Sr^{2+}-induced asynchronous IPSCs were manually detected, and their amplitudes were measured using Clampex software. Statistical comparison of uIPSC properties was performed using Student's *t*-test, unless stated otherwise. Data are presented as mean ± SE.

Following the physiological experiments, slices containing biocytin-filled neurons were processed with the standard avidin-biotin-peroxidase method described elsewhere in detail (Horikawa and Armstrong 1988; Tseng et al. 1991). The biocytin-labeled neurons were examined under the light microscope to verify their morphology and location.

Modeling

Simulations were performed within the NEURON environment (version 5.1, Hines and Carnevale 1997), and were based on a previously reconstructed P19 rat layer V neocortical pyramidal neuron (Mainen et al. 1995). Electrotonic and recording parameters were manually adjusted to reproduce the series resistance (8.8 MΩ), E_{IPSP} (−15 mV), mean resting potential (−69 mV), and membrane input resistance (205 MΩ) of recorded pyramidal neurons in this study. Resultant values of membrane resistivity (Rm) and axial resistance (Ra) were 102,000 Ω · cm^{-2} and 250 Ω · cm, respectively. A correction was added for membrane area contributed by spines (Mainen et al. 1995), membrane capacitance (Cm) was set at 0.75 μF · cm^{-2}, and the integration time step was 25 μs. IPSCs were simulated by a sum of two exponentials to give a fast rise time (<1 ms) and variable decay time at the synaptic location, which was varied along the apical dendritic stalk, 20–780 μm from the soma. Results are shown for the synapse located within the most proximal 230 μm. Only passive conductances were included in the model.

RESULTS

Kinetics of uIPSCs in FS-P and LTS-P cell pairs

Of 122 simultaneous recordings from pairs of interneurons and P cells, 6 LTS cells and 11 FS cells were found to have a functional synaptic connection with a postsynaptic pyramidal cell. Layer V FS interneurons and LTS cells exhibited distinct firing properties in response to suprathreshold depolarizing current pulses. FS cells fired a train of APs with little frequency adaptation when a suprathreshold depolarizing current step was applied under current-clamp conditions (Fig. 1*A1*), whereas LTS cells displayed characteristic low threshold spikes, known to be mediated by Ca^{2+} conductance, which could be elicited

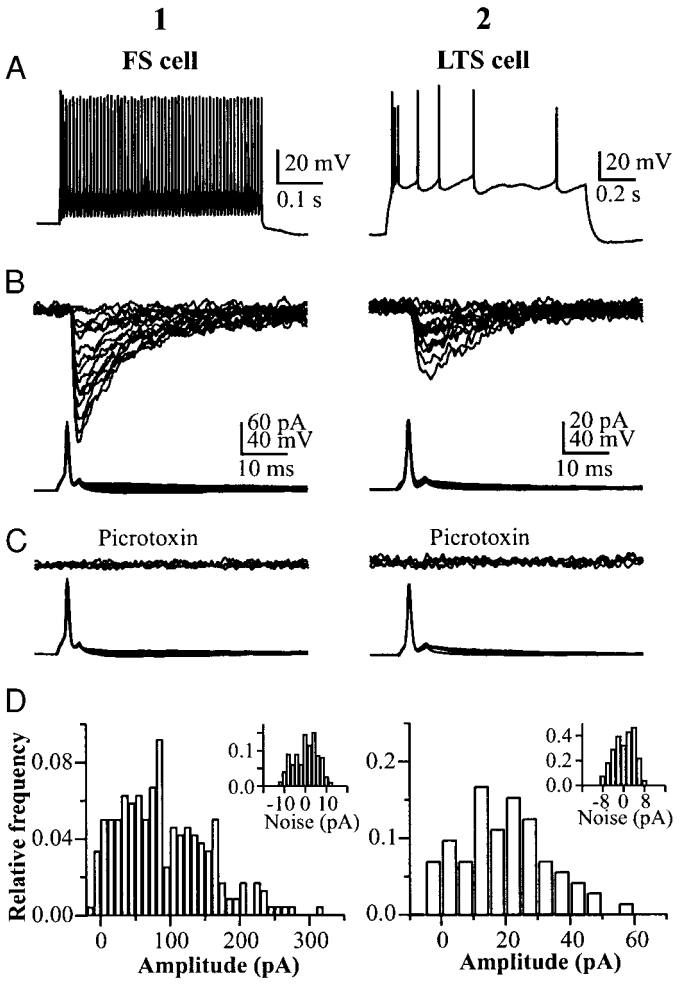

FIG. 1. Unitary inhibitory postsynaptic currents (uIPSCs) recorded from fast spiking (FS) cell-pyramidal (P) cell pairs and low-threshold spike (LTS) cell-P cell pairs. *A*: current-clamp recordings from an FS cell at a membrane potential of −58 mV (*A1*) and an LTS cell at −82 mV (*A2*) during injection of depolarizing current pulses 360 and 150 pA, respectively. *B*: postsynaptic currents recorded from a P cell (*B1, top*), while single action potentials were generated in the FS cell (*B1, bottom*), and currents recorded from another P cell (*B2, top*), while action potentials were generated in the LTS cell (*B2, bottom*). Fifteen consecutive trials shown in *B1* and *B2*. $V_h = -80$ mV for P cells in both cases. The calibration bars in *B1* and *B2* also apply to *C1* and *C2*, respectively. *C*: postsynaptic currents were blocked by application of 50 μM picrotoxin for both the FS-P cell pair (*C1*) and the LTS-P cell pair (*C2*). Five consecutive traces were superimposed in *C1* and *C2*. V_h was the same as in *B*. *D*: uIPSC amplitude and noise (*inset*) distributions from the FS-P pair of *B1* (*D1*) and the LTS-P pair of *B2* (*D2*). Distributions were constructed from 200 events for *D1* and 76 events for *D2*. Bin size was 10 pA for *D1* (*inset*, 2 pA) and 5 pA for *D2* (*inset*, 2 pA).

by a depolarizing current pulse from a hyperpolarized membrane potential (−80 mV; Fig. 1*A2*) (Foehring et al. 1991; Kawaguchi 1993; Xiang et al. 1998a). The amplitude of uIPSCs evoked in pyramidal neurons by single APs of both interneuronal types varied considerably, and transmission failures were occasionally observed in both types of synaptic connection (Fig. 1*B*). These unitary synaptic currents could be blocked by picrotoxin (50 μM), a $GABA_A$ receptor antagonist, confirming that they were $GABA_A$ receptor–mediated IPSCs (Fig. 1*C*).

The amplitude of uIPSCs for 11 individual FS-P pairs ranged from 56.2 to 650.2 pA with a mean value of 208.3 ± 58.7 pA, which was significantly larger than the value for 6 LTS-P pairs, which ranged from 20.2 to 30.8 pA with a mean value of 26.5 ± 1.6 pA ($P < 0.01$; Fig. 2*B1a*). Examples of amplitude distributions from representative FS-P and LTS-P pairs are shown in Fig. 1, *D1* and *D2*. FS cell-evoked uIPSCs had faster 10–90% rise times than those evoked by LTS cells (0.88 ± 0.06 vs. 1.42 ± 0.15 ms; $P < 0.001$; Fig. 2*B2*). These results are consistent with the anatomical observations that axons of FS cells project primarily to perisomatic areas of layer V pyramidal neurons, whereas LTS cells have more axonal arbors than FS cells in distal dendritic regions (Kawaguchi 1993; Kawaguchi and Kubota 1993; Xiang et al. 1998a) and the expected electrotonic attenuation of more distal synaptic events (Larkman et al. 1992; Spruston et al. 1994). The decay of uIPSCs for these two types of synapses could be well fit by a single exponential function (Fig. 2*A*). In contrast to the above differences in rise times, there was no significant difference in decay time constants (τ_Ds) for FS-P versus LTS-P uIPSCs, although the latter tended to decay more rapidly (τ_Ds were

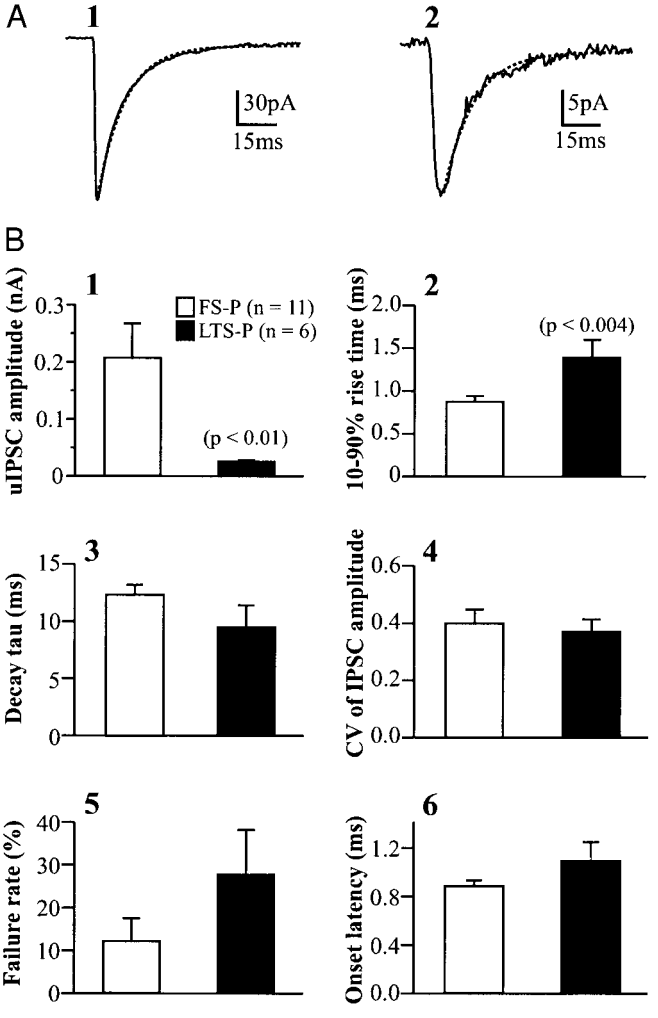

FIG. 2. Comparison of uIPSC kinetics between FS-P pairs and LTS-P pairs. *A*: examples of single exponential fits for the decay of uIPSCs evoked by an FS cell (*A1*) and an LTS cell (*A2*). Traces were averages of 10 sweeps. Dashed lines represent single exponential fitted curves. τ_D is 10.1 ms in *A1* and 7.8 ms in *A2*. *B*: bar graphs summarizing the mean values of uIPSC amplitude (*B1*), 10–90% rise times (*B2*), τ_D (*B3*), coefficient of variation (CV) of uIPSC amplitude (*B4*), failure rate (*B5*), and onset latency (*B6*).

9.4 ± 1.6 and 12.5 ± 0.8 ms for LTS-P and FS-P uIPSCs, respectively; $P > 0.05$; Fig. 2*B3*). This apparent discrepancy was explored in the modeling experiments described below. uIPSCs evoked in two different P cells by a single presynaptic interneuron had very similar kinetics ($n = 2$; Fig. 3), suggesting that the axonal terminals originating from the same interneuron might synapse onto similar somatodendritic domains of the P cells, and that $GABA_A$ receptors postsynaptic to these terminals have similar properties (Cobb et al. 1997; Gupta et al. 2000).

No significant difference in amplitude variability was found between FS-P and LTS-P uIPSCs, indicated by coefficient of variation (CV) analysis (Fig. 2*B4*; 0.40 ± 0.05 vs. 0.37 ± 0.04 for FS-P and LTS-P pairs, respectively). In general, failure rates were slightly higher for LTS-P pairs (27.9 ± 10.3% for LTS-P synapses vs. 12.3 ± 5.2% for FS-P synapses, Fig. 2*B5*) and onset latency was longer (Fig. 2*B6*; 1.09 ± 0.15 vs. 0.88 ± 0.04 ms for LTS-P and FS-P pairs, respectively), but these differences were not statistically significant. Functional reciprocal synaptic connections were detected in 2/11 FS-P pairs, but none were found in 6 LTS-P pairs.

Short-term synaptic plasticity

When a pair of APs was generated in interneurons at an interval of 50 ms, PPD of uIPSCs was observed in 4/4 LTS-P pairs and 9/10 FS-P pairs. One FS-P pair did not exhibit obvious paired-pulse modification. Examples of PPD for an FS-P cell pair and an LTP-P pair are shown in Fig. 4*A*. The mean amplitude of the second uIPSC (uIPSC2) was significantly smaller than that of the first (uIPCS1) for both types of synaptic connections (Fig. 4*B1*). Transmission failures were observed in 4/4 LTS-P pairs and 6/10 FS-P pairs that were tested with the paired-pulse protocol. Usually the second AP was less successful in evoking a uIPSC than the first one; in other words, PPD was generally associated with an increase in the failure rate (Fig. 4, *C* and *D*). Furthermore, PPD was accompanied by a decrease in CV^{-2} (Fig. 4, *E* and *F*). Together with the increase in failure rate during PPD, the results of variance analysis (Fig. 4, *E* and *F*) are in agreement with presynaptic mechanisms of PPD (Zucker 1989). The failure rate did not change during PPD in five FS-P pairs that had either a very low rate of failure (1 pair) or no failures in response to the first AP (4 pairs; Fig. 4*C*). This may be due to a large number of inhibitory synaptic contacts in these pairs.

During PPD, the peak amplitude of uIPSC2 was not significantly correlated with that of uIPSC1 at either LTS-P or FS-P synapses (Fig. 5). The correlation coefficient of the linear regression in plots of uIPSC2 versus uIPSC1 for individual pairs ranged from −0.212 to 0.295 for LTS-P pairs ($n = 4$) and from −0.376 to 0.229 for FS-P pairs ($n = 10$); none of these correlations were statistically significant (e.g., Fig. 5, *A1* and *A2*). The analysis of group data in Fig. 5*B* shows that no significant correlation was apparent between uIPSC1 and uIPSC2 peak amplitudes for either FS-P (*B1*) or LTS-P synapses (*B2*) ($P > 0.5$). Furthermore, the average amplitude of *response 2* in the trials with *response 1* failures was similar to, or smaller than, the average amplitude that followed *response 1* successes (e.g., Fig. 5*C*). These data suggested that PPD at both FS-P and LTS-P synapses was not dependent on previous release.

When multiple APs were generated in presynaptic interneurons at 20 Hz, uIPSC amplitude decreased over time at both FS-P and LTS-P synapses. The uIPSC amplitude decline could be fit by a single exponential function, and the synaptic depression dynamics were different for LTS-P versus FS-P synapses, with LTS-P uIPSC amplitudes decrementing more rapidly than those for FS-P uIPSCs (Fig. 6). The mean time constant for depression in amplitude of successive uIPSCs for LTS-P pairs was significantly shorter (58.0 ± 3.5 ms, $n = 4$) than for FS-P pairs (84.5 ± 4.5 ms, $n = 5$). The normalized amplitude of the uIPSC corresponding to the last (7th) presynaptic AP was not significantly different between these two synapses (0.32 ± 5% for LTS-P vs. 37 ± 6% for FS-P synapses; $P > 0.05$; Fig. 6*D*). This finding suggests that steady state IPSC depression at these two synapses was comparable.

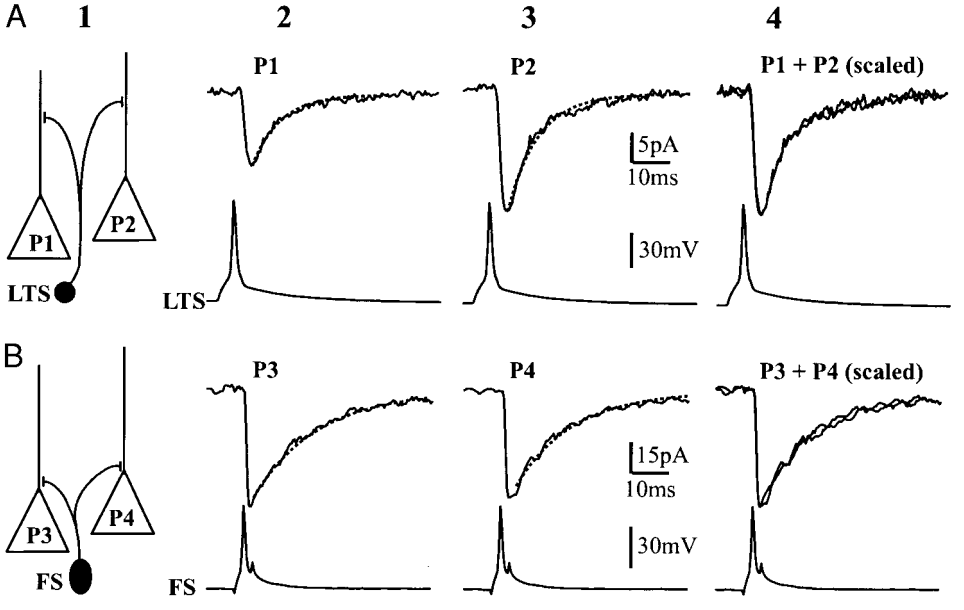

FIG. 3. Similar kinetic properties of uIPSCs evoked in different pyramidal cells by a single interneuron. *A* and *B*: schematic diagrams illustrating an LTS cell (*A1*) synapsing onto 2 adjacent P cells (P1 and P2 in *A2* and *A3*), and an FS cell (*B1*) synapsing onto 2 other pyramidal cells (P3 and P4 in *B2* and *B3*). *A2* and *A3*: average uIPSCs evoked in P1 (*A2*, *top*) and P2 (*A3*, *top*) by action potentials in the LTS cell (*A2* and *A3*, *bottom*). *A4*: P1 and P2 uIPSCs of *A2* and *A3* scaled to the same amplitude and superimposed to show their similar rise times and decay kinetics. *B2* and *B3*: average uIPSCs evoked in P3 (*B2*, *top*) and P4 (*B3*, *top*) by action potentials in the FS cell (*bottom*). *B4*: P3 and P4 uIPSCs of *B2* and *B3* scaled to the same amplitude and superimposed. Rise times (10–90%) are 1.72, 1.76, 0.86, and 0.74 ms for P1–P4, respectively. τ_Ds are 7.8, 7.4, 18.6, and 16.7 ms for P1–P4, respectively. Each trace is an average of 10–20 sweeps. Dashed lines in *A3* and *B3* are single exponential fitting curves.

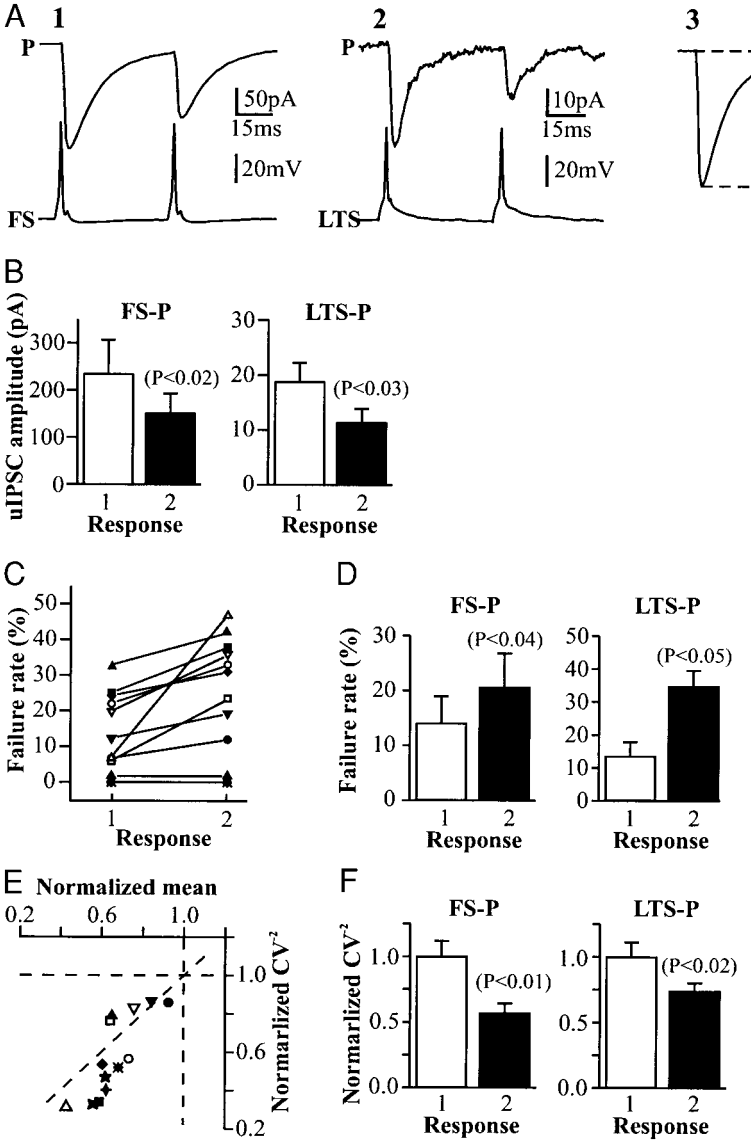

FIG. 4. Paired-pulse depression (PPD) was associated with an increase in failure rate and decrease in CV^{-2}. *A*: average uIPSCs recorded from a P cell (P) following 2 action potentials elicited in an FS cell (*A1*), and average uIPSCs from another P cell (P) following 2 action potentials elicited in an LTS cell (*A2*). Inter-spike interval was 50 ms. Current traces are an average of 10 sweeps. *A3*: measurement of peak amplitude for uIPSC1 (A_1) and uIPSC2 (A_2). *B*: bar graphs summarizing mean amplitude for *responses 1* and *2* during PPD for FS-P pairs ($n = 8$, *left*) and LTS-P pairs ($n = 4$, *right*). *C*: plot of failure rate for the first and second uIPSC during PPD. Note that an increase in failure rate is associated with PPD in most cases, and there were no failures for uIPSC1 and uIPSC2 during PPD in 4 FS-P pairs (4 horizontal lines are superimposed at 0 failure rate). *D*: bar graphs summarizing mean failure rate of *responses 1* and *2* for FS-P pairs with nonzero failures in *response 1* ($n = 5$, *left*) and LTS-P pairs ($n = 4$, *right*). *E*: plot of CV^{-2} of peak amplitude against mean amplitude. Both CV^{-2} and mean were normalized to the values of the first uIPSCs. *F*: bar graphs summarizing averaged CV^{-2} values of *responses 1* and *2* for FS-P pairs ($n = 9$, *left*) and LTS-P pairs ($n = 4$, *right*). Different symbols represent different pairs in *C* and *E*; solid symbols represent the FS-P pairs and open symbols represent LTS-P pairs.

Multiple functional synapses or release sites contribute to the uIPSCs

To assess the number of functional synapses or release sites required to account for the observed uIPSC amplitudes, we used two methods to estimate the quantal size: *1*) local application of sucrose to evoke mIPSCs (Bekkers and Stevens 1995), and *2*) addition of Sr^{2+} to the ASCF to induce asynchronous delayed release (Morishita and Alger 1997; Ohno-Shosaku et al. 1994). Because LTS cells have more vertically oriented axonal arborizations that distribute across the laminae toward the upper cortical layers (Kawaguchi 1993; Kawaguchi and Kubota 1993; Xiang et al. 1998a), they are likely to form synapses on more distal dendritic regions of P cells. Thus the uIPSCs obtained from the P cells following LTS cell APs would likely suffer varying degrees of dendritic attenuation, making it difficult to obtain a robust estimate of quantal size. Therefore our analysis was focused on FS-P synapses, which are likely to be located in perisomatic areas of layer V pyramidal neurons and to be less affected by electrotonic attenuation.

Focal application of hypertonic solution has been used to locally elicit miniature excitatory postsynaptic currents (mEPSCs) in hippocampal neurons in dissociated culture (Bekkers and Stevens 1995) and mIPSCs in neocortical layer V pyramidal neurons (Salin and Prince 1996). We adapted this technique to locally evoke mIPSCs in layer V P cells. In the presence of DNQX (20 μM), APV (50 μM), and TTX (1 μM), sucrose (1 M) was applied by a brief pressure delivered through a patch pipette positioned approximately 50 μm away from the soma of the recorded P cell. Local application of sucrose caused an increase in the frequency of mIPSCs (Fig. 7, *A1* and *A2*). The amplitude distribution of the sucrose-evoked mIPSCs was skewed to the right (Fig. 7*A3*) and presumably approximated the distribution of quantal events originating from FS-P synapses and possibly other interneuronal synapses close to the P cell somata. The mIPSC amplitude had a mean value of 22.8 $\pm$ 2.6 pA and a mean CV of 66.1 $\pm$ 7.1% ($n = 5$).

Adding Sr^{2+} to ACSF during paired recordings led to a decrease in the amplitude of evoked uIPSCs, followed by an increase in frequency of spontaneous IPSCs (sIPSCs) (Fig. 7,

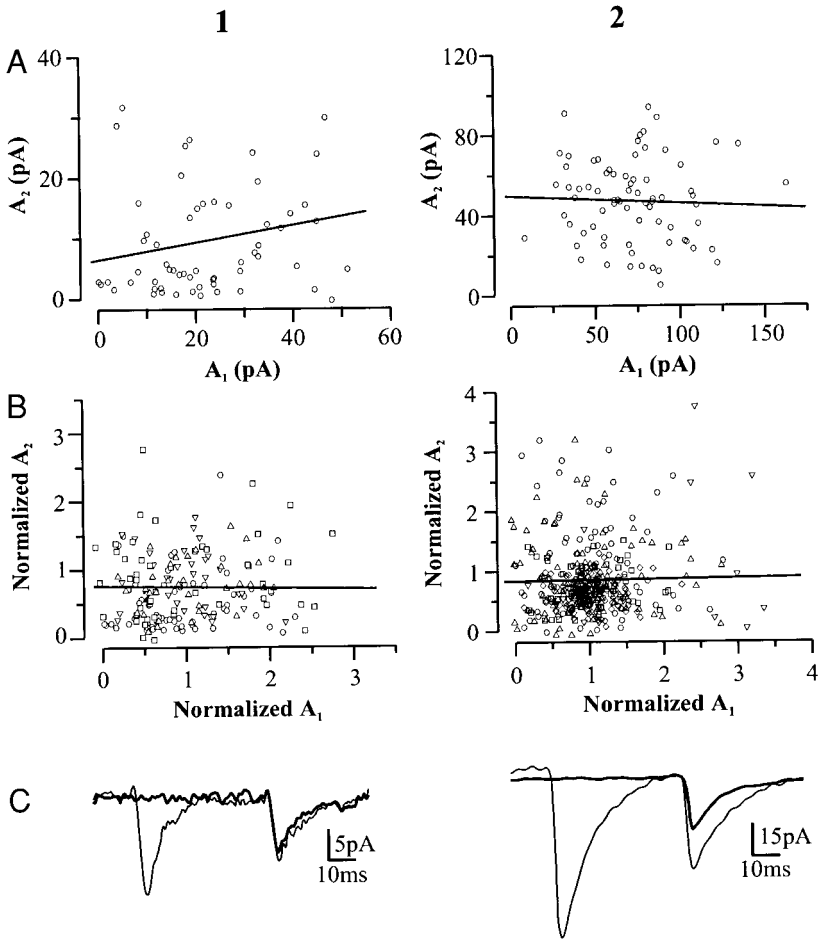

FIG. 5. PPD at LTS-P and FS-P synapses appears to be independent of the previous release. *A*: plot of peak amplitude of uIPSC2 (A_2) vs. uIPSC1 (A_1) for individual events from an LTS-P pair (*A1*) and an FS-P pair (*A2*). Lines represent the results of linear regression. Correlation coefficient is 0.177 ($P = 0.176$) for *A1* and −0.05 ($P = 0.663$) for *A2*. *B*: plot of normalized amplitude of uIPSC2 against uIPSC1 for a group of 4 LTS-P pairs (*B1*) and a group of 10 FS-P pairs (*B2*). Amplitudes were normalized to the mean value of uIPSC1 for each pair. Different symbols represent the different pairs. Lines are the results of linear regression. Correlation coefficient is −0.017 ($P = 0.823$) for *B1* and 0.0134 ($P = 0.779$) for *B2*. *C*: comparison of averaged IPSCs with *response 1* failures (thick lines) and those with *response 1* successes (thin lines) for an LTS-P pair (*C1*) and an FS-P pair (*C2*). Each trace was an average of 8–55 sweeps.

B1 and *B2*). In the control condition, mean value of sIPSC frequency was 1.6 ± 0.4 Hz ($n = 3$), similar to that reported in our previous study (Xiang et al. 1998b). After Sr^{2+} was added to ACSF, the frequency of sIPSCs in the 400-ms period following uIPSCs increased to 5.0 ± 0.7 Hz ($n = 3$). These Sr^{2+}-dependent spontaneous events are believed to result from delayed asynchronous release of the transmitter from the terminals of the neuron being activated and have features resem-

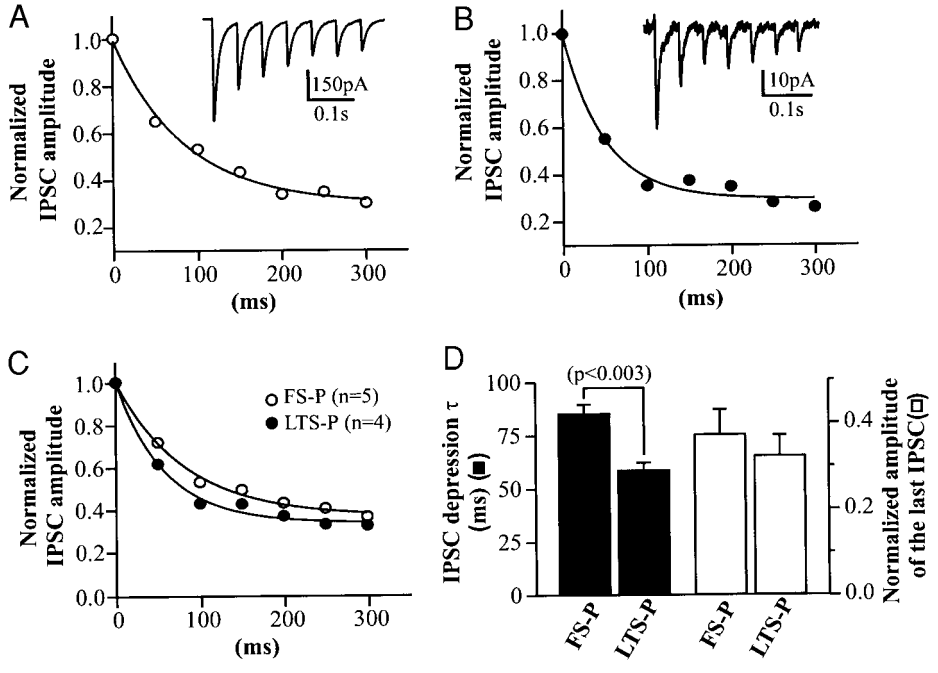

FIG. 6. Difference in short-term synaptic dynamics of FS-P cell synapses and LTS-P cell synapses. *A*: normalized uIPSC amplitudes in a P cell elicited by a train of 7 action potentials (APs) in an FS cell at 20 Hz. *Inset*: averaged uIPSCs from the P cell in response to trains of the FS cell APs. *B*: normalized uIPSC amplitudes in another P cell evoked by a train of APs in an LTS cell at 20 Hz. *Inset*: averaged uIPSCs from the P cell in response to trains of the LTS cell APs. Solid lines in *A* and *B* represent single exponential fits to the decline of the uIPSC amplitudes. τ is 90.0 ms in *A* and 49.6 ms in *B*. *C*: average normalized uIPSC amplitudes plotted against time for FS-P pairs (open symbols) and LTS-P pairs (closed symbols). Solid lines represent the single exponential fitted curves. τ is 83.1 ms for FS-P pairs and 58.4 ms for LTS-P pairs. *D*: bar graph summarizing the group data of uIPSC amplitude decay time constants (solid bars) and normalized steady state values (open bars) for FS-P pairs ($n = 5$) and LTP-P pairs ($n = 4$).

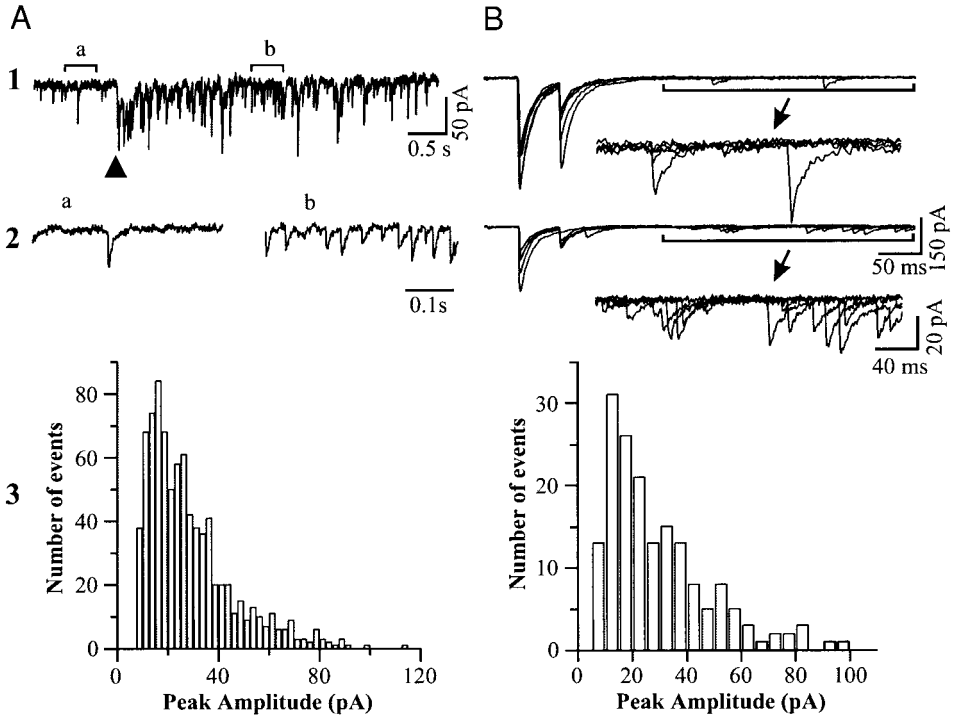

FIG. 7. Estimate of quantal size of FS-P synapses by focal application of sucrose or addition of Sr^{2+} to artificial cerebrospinal fluid (ACSF). *A*: analysis of miniature IPSCs (mIPSCs) evoked by sucrose application. *A1*: example of mIPSCs recorded from a P cell before and after application of 1 M sucrose delivered by a brief pressure pulse through a patch pipette positioned at ~ 50 μm away from the soma. Arrowhead indicates the time of sucrose application. *A2*, a and b: segments a and b of trace of *A1*, displayed at a faster time scale to show mIPSCs before (a) and after (b) sucrose application. *A3*: peak amplitude distribution histogram of mIPSCs for the cell in *A1*. *B*: analysis of spontaneous IPSCs evoked in Sr^{2+}-containing ACSF. *B1*: 5 superimposed traces of uIPSCs recorded from a P cell following 2 APs elicited in an FS cell at an inter-spike interval of 50 ms, in control ACSF containing 2 mM Ca^{2+} and 2 mM Mg^{2+}. *Inset*: segment of traces marked by bracket in *top trace* displayed at higher gain. Calibrations for *B1* in *B2*. *B2*: 5 superimposed traces of uIPSCs from the same pair as in *B1* in the presence of 4 mM Sr^{2+}. *Inset*: segment of traces marked by bracket in *top trace* displayed at higher gain. Note that in the presence of Sr^{2+}, amplitude of synchronous uIPSCs evoked by the FS interneuron was reduced, followed by an increase in frequency of delayed spontaneous synaptic events. *B3*: amplitude distribution of delayed spontaneous IPSCs for the same cell as in *B1* and *B2*.

bling miniature synaptic events (Goda and Stevens 1994; Morishita and Alger 1997; Ohno-Shosaku et al. 1994). The amplitude distributions of evoked asynchronous sIPSCs in the presence of Sr^{2+} were also skewed toward larger amplitudes (Fig. 7*B3*). The Sr^{2+}-induced sIPSC amplitude had a mean value of 24.3 ± 6.2 pA and a mean CV of 48.1 ± 8.1% (n = 3), very similar to values for sucrose-evoked mIPSCs (cf. Fig. 7, *A3* and *B3*). These results suggest that delayed sIPSCs following uIPSCs, in the presence of Sr^{2+}, are miniature-like events and likely to arise from asynchronous release of the transmitter from the axonal terminals of FS cells.

For the mIPSCs induced by focal application of hypertonic sucrose solution or by adding Sr^{2+} to external bathing solution during the paired recordings, the amplitude distributions were always positively skewed. If we assume that the mean value of mIPSC (or Sr^{2+}-induced sIPSC) amplitude reflects the postsynaptic responses produced by one vesicle released from a single synapse or release site (see DISCUSSION), then the uIPSCs in P cells evoked by single APs in FS cells (complete amplitude range of 19–1,108 pA) could result from the activation of approximately 1–48 synapses or release sites. With mean uIPSC amplitudes for the 11 individual FS-P pairs ranging from 56.2 to 650.2 pA, we estimated that, on average, synchronous activation of 2–28 synapses or release sites was required to produce the unitary postsynaptic currents.

Simulations of FS-P and LTS-P synapses

To assess the role of electrotonic attenuation in the apparent differences in the kinetics of FS-P versus LTS-P IPSCs mentioned above, we simulated synaptic inputs with varying time courses and at different locations along the somatodendritic tree. We used a previously reconstructed and modeled layer V pyramidal neuron (Mainen et al. 1995) that was of similar developmental stage to that used in the present study. The model parameters were adjusted so that the simulated neuron had electrotonic properties relevant to the recordings of IPSCs in pyramidal neurons (see METHODS). We tested whether a common synaptic conductance waveform could be injected at two different synaptic sites on the model pyramidal neuron and produce resultant voltage-clamp current waveforms consistent with FS-P versus LTS-P synapses. IPSC conductance waveforms had a rise time of 0.1 ms and decay time constants varying between 2 and 14 ms. Results of the simulations are shown in Fig. 8, where measured rise times and decay time constants are shown for the various simulations.

Initially we performed a series of simulations in which we varied axial resistance (Ra, 80–400 $\Omega \cdot$ cm) to arrive at a simulated pyramidal neuron that gave realistic results, including IPSCs with rise times <1 ms, and decay times consistent with FS-P responses. A value of 250 $\Omega \cdot$ cm provided results

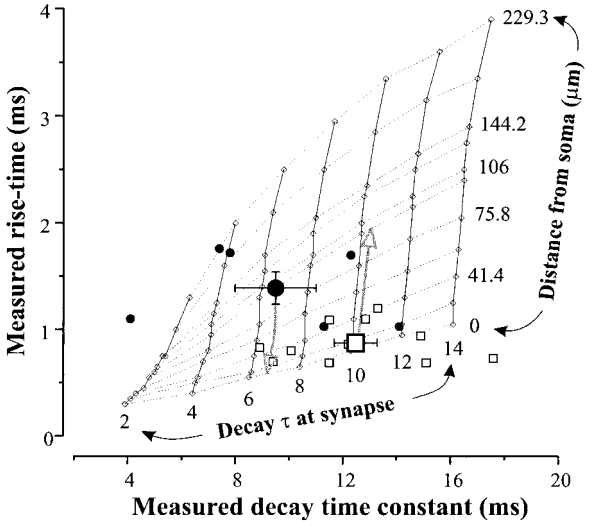

FIG. 8. Simulations of recorded IPSCs in a layer V pyramidal neuron. Synapses with a range of decay time constants (2–14 ms, "Decay τ at synapse") were inserted at various locations along the shaft of the main apical dendrite (0–229.3 μm; "Distance from soma"). The simulated somatic whole cell IPSC was obtained, and its kinetics analyzed to obtain a "measured" rise-time and decay time constant. Vertical lines indicate IPSC parameters for equivalent synaptic conductance waveforms inserted into different dendritic locations, while horizontal dashed lines indicate parameters for varying conductance waveforms inserted at a given location. □, experimental values obtained for FS-P pairs; ●, experimental values obtained from LTS-P pairs. Large symbols (□, ●) are the mean responses of each population, with error bars indicating SE. Note that for these simulations, FS synapses fall in a cluster near the soma, while LTS synapses are located approximately 20–230 μm from the soma. Gray open arrows, recorded IPSC kinetics (decay $\tau \approx 13$ ms, rise-time ≈ 2 ms) if the mean FS-P synapse was to be moved approximately 100 μm out into the apical dendrite, or if the LTS-P synapses were to be moved to the soma (decay $\tau \approx 9$ ms, rise-time ≈ 0.6 ms).

that were consistent with the expected behavior of FS-P synapses, which, from reconstructions of FS cell axonal branches, should be largely somatic (Xiang et al. 1998a; Fig. 8, small □ symbols). This neuronal structure produced a mean LTS-P IPSC (Fig. 8, large ●) with a decay time constant of about 6 ms at the synapse, a recorded rise time of >1 ms, and a location about 90 μm from the soma. This is consistent with the putative location of LTS-P synapses centered at >100 μm from the soma (Xiang et al. 1998a; see also Tamas et al. 1997). The results of these simulations are inconsistent with the null hypothesis that an equivalent $GABA_A$ receptor–mediated synaptic conductance could underlie both LTS-P and FS-P responses. This overall result was confirmed in a number of simulations in which we varied basic model parameters, including overall cell length, series resistance, spine membrane correction (see METHODS), and rise time of the synaptic conductance.

What would be the time course of a LTS-P IPSC, if the underlying conductance waveform were equivalent to that of an FS-P connection? The arrows in Fig. 8 illustrate this result. If the FS-P synapse were to be moved out to the dendrite, it would have a slightly slower decay time constant and a much slower (>2×) rise time. These values are inconsistent with the IPSC kinetics obtained in the LTS-P recordings. By contrast, if the mean LTS-P synapse were moved to the soma, the recorded IPSC would decay much more rapidly than the measured FS-P response. The near vertical lines in the grid indicate the expected differences in recorded IPSC as a given synaptic waveform is moved out along the dendrite. In general these lines have positive slopes, i.e., as the synapse is made more distant, both the rise time and decay time constant increase. Negative slopes were never obtained in any simulations. Thus given a fixed time-course $GABA_A$ receptor–mediated conductance, it is impossible to move from the mean FS-P to the mean LTS-P IPSC. Of the 11 FS cells (shown as small □), 10 are located to the right of the descending gray arrow that indicates the expected IPSC kinetics when a distal LTS-P synapse is moved toward the soma. Similarly, five of the six LTS-P IPSCs (small ●) fell to the left of the synaptic waveform expected if a typical fast spiking synapse were moved 100 μm into the dendrites (ascending gray arrow).

DISCUSSION

Our results demonstrate that uIPSCs generated in P cells by two physiologically and morphologically distinct subtypes of interneurons are mediated by $GABA_A$ receptors, with kinetics that depend on the type of presynaptic cell. uIPSCs at LTS-P cell synapses were smaller in amplitude and had slower rise times than those at FS-P cell synapses, consistent with anatomical observations that the two types of synapses are likely located on different somato-dendritic domains of the P cells (Deuchars and Thomson 1995; Kawaguchi 1993; Tamas et al. 1997; Thomson et al. 1996; Xiang et al. 1998a) and the expected electrotonic attenuation of more distal synaptic events (Larkman et al. 1992; Spruston et al. 1994). Differences in amplitudes and rise times of uIPSCs, evoked on pyramidal neurons by subclasses of interneurons that have proximal versus more distal cell surface domains, are present in hippocampus (Maccaferri et al. 2000; Ouardouz and Lacaille 1997). However, in contrast to the results of these hippocampal experiments, τ_D of presumably distal LTS-P uIPSCs in our experiments was not significantly different from that of more proximal FS-P uIPSCs. This finding is contrary to the assumption that distal synaptic events should have both a slower rise and a slower decay due to dendritic filtering. If the functional properties of $GABA_A$ receptors were the same at these two synapses, we would expect a slightly longer τ_D and much longer rise time for LTS-P uIPSCs (Fig. 8). One possible explanation for the apparent discrepancy would be differences in the properties of $GABA_A$ receptors at LTS-P versus FS-P synapses. Such cell type–specific differences might be due to variations in $GABA_A$ receptor–subunit composition at these two synapses (Maccaferri et al. 2000; Nusser et al. 1996; Nyiri et al. 2001) and/or differential regulation of $GABA_A$ receptors by, for example, phosphorylation (McDonald et al. 1998; Nusser et al. 1999). Alternatively, the slow rise time could be caused by asynchronous vesicular release at multiple contacts of an LTS-P pair. The finding that rise times were slow for even the smallest events, which were likely evoked by single quanta (unpublished observations), argues against the this possibility. A less likely possibility is that the ISPC variations were due to differences in GABA uptake, which has been shown to regulate IPSP duration in some circumstances (Thompson and Gähwiler 1992).

To estimate the number of synaptic contacts mediating uIPSCs, the size of the response at each contact must be determined. This is usually obtained from the distribution of mIPSC amplitudes, using either overall mean or amplitude of

the first peak in the distribution (Bekkers and Clements 1999; Cox et al. 1997; Edwards et al. 1990; Frerking et al. 1997; Paulsen and Heggelund 1996). As there is no consensus regarding the biological basis for the skewed distributions of miniature synaptic current amplitudes (Fig. 7, *A3* and *B3*), we have used the mean rather than first peak amplitude. Skewed distributions have been observed at excitatory as well as inhibitory synapses in various preparations, even under recording conditions where dendritic filtering is minimal (Bekkers and Clements 1999; Bekkers and Stevens 1995; Korn et al. 1993; Legendre and Korn 1994; Vautrin and Barker 1995). Two main hypotheses have been proposed: *1*) such skew may result from multivesicular release from single terminals, especially from those with more than one active zone (Korn et al. 1993; Legendre and Korn 1994; Vautrin and Barker 1995) or *2*) such skew may be due to quantal variance within a synaptic site (Bekkers and Stevens 1995; Frerking and Wilson 1996). The results from more recent studies have favored the second hypothesis (Bekkers and Clements 1999; Frerking et al. 1997).

Based on our electrophysiological data, we estimated that, on average, synchronous activation of 2–28 synapses or release sites was required to produce the FS-P unitary postsynaptic currents observed in these experiments. In a previous study in adult rat somatomotor cortex, cell morphology was fully reconstructed after paired recordings from cortical FS and P cells (Thomson et al. 1996). Three and five synaptic contacts were identified after reconstruction of presynaptic layer V FS cells and postsynaptic layers II and V P cells, respectively; the associated uIPSPs were small (amplitude ~0.24 mV on average, at membrane potentials of −55 to −60 mV). Larger amplitude uIPSPs (2.2 mV on average), which might reflect larger numbers of synaptic contacts, were also observed in other FS-P pairs under similar conditions (Thomson et al. 1996). A simple calculation from the numbers cited above suggests that the large amplitude uIPSPs in the FS-P pairs of the Thomson et al. (1996) study might involve approximately 30–50 synapses or release sites on average, similar to our upper estimate for the number of FS-P synapses underlying the average uIPSC amplitude. The actual number of functional synapses or release sites for FS-P pairs could be even higher because release probability for individual synapses is usually <1.

Under our recording conditions (V_h = −80 mV, high Cl^- concentration in the patch pipette and calculated E_{Cl} of −15 mV), we estimated that the mean quantal size for FS-P synapses was ~23 pA, equivalent to an apparent quantal conductance of 0.35 nS. Single channel conductance of $GABA_A$ receptors in layer V pyramidal neurons of rat visual cortex was estimated to be approximately 15 pS with cell-attached recordings (Xiang et al. 1998b) and approximately 25 pS when outside-out patch recordings were used (Perrais and Ropert 1999). Cell-attached recordings seem to yield lower conductance values for GABA-activated single Cl^- channels than outside-out recordings, for example, 17 versus 30 pS in spinal cord neurons (Bormann et al. 1987). If the single channel conductance for $GABA_A$ receptors in the P cell is assumed to be approximately 25 pS, there would be, on average, 14 $GABA_A$ receptor channels opening at the peak of a quantal IPSC at FS-P cell synapses.

The uIPSC amplitude in P cells following a single AP in FS cells was significantly larger than that following a LTS cell AP. We assume that this is mainly due to the fact that FS cells have a larger number of release sites located in the perisomatic area of pyramidal neurons than do LTS cells. Other possibilities still remain to be addressed, such as potential differences in $GABA_A$ receptor conductance and number/density at proximal versus distal dendritic sites on the P cells. The larger amplitude of FS cell-evoked uIPSCs is not likely to result from simultaneous firing of multiple electrically coupled FS cells, as the coupling ratio for APs between two FS cells in the neocortex is very small (Galarreta and Hestrin 1999; Gibson et al. 1999).

Synaptic depression has been attributed to both presynaptic and postsynaptic mechanisms, with the most common hypotheses being negative feedback mediated by presynaptic $GABA_B$ receptors (Deisz and Prince 1989; Lambert and Wilson 1994), desensitization of postsynaptic receptors (Jones and Westbrook 1996), and depletion of the releasable pool of synaptic vesicles (Debanne et al. 1996; Dobrunz and Stevens 1997). However none of these mechanisms appear to be primarily responsible for PPD of uIPSCs at the FS-P and LTS-P synapses. Presynaptic receptors do not appear to be involved, because PPD was not affected by $GABA_B$ receptor antagonists at LTS-P cell synapses in the neocortex (Deuchars and Thomson 1995) and interneuron-principal cell synapses in the hippocampus (Bertrand and Lacaille 2001; Jiang et al. 2000; Kraushaar and Jonas 2000). Desensitization of postsynaptic $GABA_A$ receptors is not the major factor underlying PPD, because failure and CV analyses suggested that the primary locus of PPD is presynaptic (Fig. 4). Vesicle pool depletion also seems to be unlikely, because an expected negative correlation between the amplitudes of the second and first uIPSCs (Jiang et al. 2000) was not observed (Fig. 5). This independence of PPD on previous release also argues against both desensitization of postsynaptic $GABA_A$ receptors and activation of presynaptic $GABA_B$ receptors. A similar release-independent PPD has also been reported at other sites, such as inhibitory synapses in the dentate gyrus (Kraushaar and Jonas 2000), excitatory synapses in the cortex (Thomson and Bannister 1999), CA1 area of the hippocampus (Dobrunz et al. 1997), and calyceal synapses in the auditory pathway at the endbulb of Held (Bellingham and Walmsley 1999).

Possible mechanisms underlying the release-independent PPD include decrease in vesicle release probability after the first spike (Betz 1970), increase in probability of branch-point failure for conduction of the second AP (Brody and Yue 2000; Luscher and Shiner 1990; but see Cox et al. 2000), activity-dependent inactivation of presynaptic Ca^{2+} channels (Patil et al. 1998), and reduction of Ca^{2+} influx resulting from changes in amplitude of presynaptic APs (Hawkins et al. 1983). Another possibility could be release of a second transmitter with presynaptic inhibitory actions, such as neuropeptide Y (NPY) (Sun et al. 2001). Subsets of cortical FS and LTS cells contain NPY (Cauli et al. 1997), and NPY has been shown to inhibit glutamate release in the hippocampus (Qian et al. 1997) and $GABA_A$ receptor–mediated transmission in suprachiasmatic nucleus neuron culture (Chen and van den Pol 1996) and in thalamic slices (Sun et al. 2001), through its action at presynaptic sites. Additional experiments are required to further investigate these possible mechanisms.

During a short train of action potentials in presynaptic interneurons, uIPSC amplitude at both FS-P and LTS-P cell synapses declined exponentially (Fig. 6), and more slowly for FS-P than for LTS-P uIPSCs. The mechanisms underlying this

form of short-term synaptic plasticity are not completely understood. They may be similar to those suggested above for PPD, but different from the slow component of depression during a long train of APs (Galarreta and Hestrin 1998; Kraushaar and Jonas 2000). In any case, the precise biophysical and molecular basis for this type of synaptic depression remains to be further investigated.

In summary, LTS and FS inhibitory interneurons have different synaptic connectivities to P cells, with LTS cells possibly having more synapses impinging onto distal dendrites, and FS cells having more perisomatic synapses. This implies that these two subtypes of interneurons play different roles in the functional operation of the cortex. LTS cells may influence the input-output characteristics of pyramidal neurons by shunting excitatory dendritic currents and/or by reducing the activation of voltage- dependent Na^+ channels and high-voltage activated Ca^{2+} channels that are present in apical dendrites of layer V pyramidal cells (Huguenard et al. 1989; Markram et al. 1995; Stuart and Sakmann 1994). On the other hand, FS cells that have multiple synapses on the perisomatic area could directly control the excitability of a pyramidal neuron by evoking shunting inhibition, and possibly hyperpolarization in the soma and proximal dendrites, and thus filtering the integrated output of the neuron by altering the spike firing pattern (Somogyi et al. 1998; Thomson et al. 1996).

We thank I. Parada for excellent assistance.

This work was supported by the Pimley Research and Training Funds and National Institutes of Neurological Disorders and Stroke Grants NS-12151 and NS-07280.

REFERENCES

BARKER JL AND HARRISON NL. Outward rectification of inhibitory postsynaptic currents in cultured rat hippocampal neurones. *J Physiol (Lond)* 403: 41–55, 1988.

BEKKERS JM AND CLEMENTS JD. Quantal amplitude and quantal variance of strontium-induced asynchronous EPSCs in rat dentate granule neurons. *J Physiol (Lond)* 516: 227–248, 1999.

BEKKERS JM AND STEVENS CF. Quantal analysis of EPSCs recorded from small numbers of synapses in hippocampal cultures. *J Neurophysiol* 73: 1145–1156, 1995.

BELLINGHAM MC AND WALMSLEY B. A novel presynaptic inhibitory mechanism underlies paired pulse depression at a fast central synapse. *Neuron* 23: 159–170, 1999.

BERTRAND S AND LACAILLE JC. Unitary synaptic currents between lacunosum-moleculare interneurones and pyramidal cells in rat hippocampus. *J Physiol (Lond)* 532: 369–384, 2001.

BETZ WJ. Depression of transmitter release at the neuromuscular junction of the frog. *J Physiol (Lond)* 206: 629–644, 1970.

BORMANN J, HAMILL OP, AND SAKMANN B. Mechanism of anion permeation through channels gated by glycine and gamma-aminobutyric acid in mouse cultured spinal neurones. *J Physiol (Lond)* 385: 243–286, 1987.

BRODY DL AND YUE DT. Release-independent short-term synaptic depression in cultured hippocampal neurons. *J Neurosci* 20: 2480–2494, 2000.

CAULI B, AUDINAT E, LAMBOLEZ B, ANGULO MC, ROPERT N, TSUZUKI K, HESTRIN S, AND ROSSIER J. Molecular and physiological diversity of cortical nonpyramidal cells. *J Neurosci* 17: 3894–3906, 1997.

CHEN G AND VAN DEN POL AN. Multiple NPY receptors coexist in pre- and postsynaptic sites: inhibition of GABA release in isolated self-innervating SCN neurons. *J Neurosci* 16: 7711–7724, 1996.

COBB SR, HALASY K, VIDA I, NYIRI G, TAMÁS G, BUHL EH, AND SOMOGYI P. Synaptic effects of identified interneurons innervating both interneurons and pyramidal cells in the rat hippocampus. *Neuroscience* 79: 629–648, 1997.

COX CL, DENK W, TANK DW, AND SVOBODA K. Action potentials reliably invade axonal arbors of rat neocortical neurons. *Proc Natl Acad Sci USA* 97: 9724–9728, 2000.

COX CL, HUGUENARD JR, AND PRINCE DA. Nucleus reticularis neurons mediate diverse inhibitory effects in thalamus. *Proc Natl Acad Sci USA* 94: 8854–8859, 1997.

DEBANNE D, GUERINEAU NC, GAHWILER BH, AND THOMPSON SM. Paired-pulse facilitation and depression at unitary synapses in rat hippocampus: quantal fluctuation affects subsequent release. *J Physiol (Lond)* 491: 163–176, 1996.

DEFELIPE J, HENDRY SH, AND JONES EG. Synapses of double bouquet cells in monkey cerebral cortex visualized by calbindin immunoreactivity. *Brain Res* 503: 49–54, 1989.

DEISZ RA AND PRINCE DA. Frequency-dependent depression of inhibition in guinea-pig neocortex in vitro by $GABA_B$ receptor feed-back on GABA release. *J Physiol (Lond)* 412: 513–541, 1989.

DEUCHARS J AND THOMSON AM. Single axon fast inhibitory postsynaptic potentials elicited by a sparsely spiny interneuron in rat neocortex. *Neuroscience* 65: 935–942, 1995.

DOBRUNZ LE, HUANG EP, AND STEVENS CF. Very short-term plasticity in hippocampal synapses. *Proc Natl Acad Sci USA* 94: 14843–14847, 1997.

DOBRUNZ LE AND STEVENS CF. Heterogeneity of release probability, facilitation, and depletion at central synapses. *Neuron* 18: 995–1008, 1997.

EDWARDS FA, KONNERTH A, AND SAKMANN B. Quantal analysis of inhibitory synaptic transmission in the dentate gyrus of rat hippocampal slices: a patch-clamp study. *J Physiol (Lond)* 430: 213–249, 1990.

FOEHRING RC, LORENZON NM, HERRON P, AND WILSON CJ. Correlation of physiologically and morphologically identified neuronal types in human association cortex in vitro. *J Neurophysiol* 66: 1825–1837, 1991.

FRERKING M, BORGES S, AND WILSON M. Are some minis multiquantal? *J Neurophysiol* 78: 1293–1304, 1997.

FRERKING M AND WILSON M. Saturation of postsynaptic receptors at central synapses? *Curr Opin Neurobiol* 6: 395–403, 1996.

GALARRETA M AND HESTRIN S. Frequency-dependent synaptic depression and the balance of excitation and inhibition in the neocortex. *Nature Neurosci* 1: 587–594, 1998.

GALARRETA M AND HESTRIN S. A network of fast-spiking cells in the neocortex connected by electrical synapses. *Nature* 402: 72–75, 1999.

GIBSON JR, BEIERLEIN M, AND CONNORS BW. Two networks of electrically coupled inhibitory neurons in neocortex. *Nature* 402: 75–79, 1999.

GODA Y AND STEVENS CF. Two components of transmitter release at a central synapse. *Proc Natl Acad Sci USA* 91: 12942–12946, 1994.

GUPTA A, WANG Y, AND MARKRAM H. Organizing principles for a diversity of GABAergic interneurons and synapses in the neocortex. *Science* 287: 273–278, 2000.

HAWKINS RD, ABRAMS TW, CAREW TJ, AND KANDEL ER. A cellular mechanism of classical conditioning in Aplysia: activity-dependent amplification of presynaptic facilitation. *Science* 219: 400–405, 1983.

HENDRY SH, JONES EG, DEFELIPE J, SCHMECHEL D, BRANDON C, AND EMSON PC. Neuropeptide-containing neurons of the cerebral cortex are also GABAergic. *Proc Natl Acad Sci USA* 81: 6526–6530, 1984.

HENDRY SH, JONES EG, EMSON PC, LAWSON DE, HEIZMANN CW, AND STREIT P. Two classes of cortical GABA neurons defined by differential calcium binding protein immunoreactivities. *Exp Brain Res* 76: 467–472, 1989.

HINES M AND CARNEVALE NT. The NEURON simulation environment. *Neural Comp* 9: 1179–1209, 1997.

HORIKAWA K AND ARMSTRONG WE. A versatile means of intracellular labeling: injection of biocytin and its detection with avidin conjugates. *J Neurosci Methods* 25: 1–11, 1988.

HOUSER CR, HENDRY SH, JONES EG, AND VAUGHN JE. Morphological diversity of immunocytochemically identified GABA neurons in the monkey sensory-motor cortex. *J Neurocytol* 12: 617–638, 1983.

HUGUENARD JR, HAMILL OP, AND PRINCE DA. Sodium channels in dendrites of rat cortical pyramidal neurons. *Proc Natl Acad Sci USA* 86: 2473–2477, 1989.

JIANG L, SUN S, NEDERGAARD M, AND KANG J. Paired-pulse modulation at individual GABAergic synapses in rat hippocampus. *J Physiol (Lond)* 523: 425–439, 2000.

JONES BE AND HENDRY SH. Basket cells. In: *Cerebral Cortex*, edited by Peters A and Jones EG. New York: Plenum, 1984, p. 309–336.

JONES MV AND WESTBROOK GL. The impact of receptor desensitization on fast synaptic transmission. *Trends Neurosci* 19: 96–101, 1996.

KAWAGUCHI Y. Groupings of nonpyramidal and pyramidal cells with specific physiological and morphological characteristics in rat frontal cortex. *J Neurophysiol* 69: 416–431, 1993.

KAWAGUCHI Y AND KUBOTA Y. Correlation of physiological subgroupings of nonpyramidal cells with parvalbumin- and calbindinD28k-immunoreactive neurons in layer V of rat frontal cortex. *J Neurophysiol* 70: 387–396, 1993.

KAWAGUCHI Y, WILSON CJ, AUGOOD SJ, AND EMSON PC. Striatal interneurones: chemical, physiological and morphological characterization. *Trends Neurosci* 18: 527–535, 1995.

KORN H, BAUSELA F, CHARPIER S, AND FABER DS. Synaptic noise and multiquantal release at dendritic synapses. *J Neurophysiol* 70: 1249–1254, 1993.

KRAUSHAAR U AND JONAS P. Efficacy and stability of quantal GABA release at a hippocampal interneuron-principal neuron synapse. *J Neurosci* 20: 5594–5607, 2000.

LAMBERT NA AND WILSON WA. Temporally distinct mechanisms of use-dependent depression at inhibitory synapses in the rat hippocampus in vitro. *J Neurophysiol* 72: 121–130, 1994.

LARKMAN AU, MAJOR G, STRATFORD KJ, AND JACK JJ. Dendritic morphology of pyramidal neurones of the visual cortex of the rat. IV: Electrical geometry. *J Comp Neurol* 323: 137–152, 1992.

LEGENDRE P AND KORN H. Glycinergic inhibitory synaptic currents and related receptor channels in the zebrafish brain. *Eur J Neurosci* 6: 1544–1557, 1994.

LUSCHER HR AND SHINER JS. Computation of action potential propagation and presynaptic bouton activation in terminal arborizations of different geometries. *Biophys J* 58: 1377–1388, 1990.

MACCAFERRI G, ROBERTS JD, SZUCS P, COTTINGHAM CA, AND SOMOGYI P. Cell surface domain specific postsynaptic currents evoked by identified GABAergic neurones in rat hippocampus in vitro. *J Physiol (Lond)* 524: 91–116, 2000.

MAGEE JC AND COOK EP. Somatic EPSP amplitude is independent of synapse location in hippocampal pyramidal neurons. *Nature Neurosci* 3: 895–903, 2000.

MAINEN ZF, JOERGES J, HUGUENARD JR, AND SEJNOWSKI TJ. A model of spike initiation in neocortical pyramidal neurons. *Neuron* 15: 1427–1439, 1995.

MARKRAM H, HELM PJ, AND SAKMANN B. Dendritic calcium transients evoked by single back-propagating action potentials in rat neocortical pyramidal neurons. *J Physiol (Lond)* 485: 1–20, 1995.

MCDONALD BJ, AMATO A, CONNOLLY CN, BENKE D, MOSS SJ, AND SMART TG. Adjacent phosphorylation sites on $GABA_A$ receptor beta subunits determine regulation by cAMP-dependent protein kinase. *Nature Neurosci* 1: 23–28, 1998.

MORISHITA W AND ALGER BE. Sr^{2+} supports depolarization-induced suppression of inhibition and provides new evidence for a presynaptic expression mechanism in rat hippocampal slices. *J Physiol (Lond)* 505: 307–317, 1997.

NUSSER Z, SIEGHART W, BENKE D, FRITSCHY JM, AND SOMOGYI P. Differential synaptic localization of two major gamma-aminobutyric acid type A receptor alpha subunits on hippocampal pyramidal cells. *Proc Natl Acad Sci USA* 93: 11939–11944, 1996.

NUSSER Z, SIEGHART W, AND MODY I. Differential regulation of synaptic $GABA_A$ receptors by cAMP-dependent protein kinase in mouse cerebellar and olfactory bulb neurones. *J Physiol (Lond)* 521: 421–435, 1999.

NYIRI G, FREUND TF, AND SOMOGYI P. Input-dependent synaptic targeting of alpha(2)-subunit-containing GABA(A) receptors in synapses of hippocampal pyramidal cells of the rat. *Eur J Neurosci* 13: 428–442, 2001.

OHNO-SHOSAKU T, SAWADA S, HIRATA K, AND YAMAMOTO C. A comparison between potencies of external calcium, strontium and barium to support GABAergic synaptic transmission in rat cultured hippocampal neurons. *Neurosci Res* 20: 223–229, 1994.

OUARDOUZ M AND LACAILLE JC. Properties of unitary IPSCs in hippocampal pyramidal cells originating from different types of interneurons in young rats. *J Neurophysiol* 77: 1939–1949, 1997.

PATIL PG, BRODY DL, AND YUE DT. Preferential closed-state inactivation of neuronal calcium channels. *Neuron* 20: 1027–1038, 1998.

PAULSEN O AND HEGGELUND P. Quantal properties of spontaneous EPSCs in neurones of the guinea-pig dorsal lateral geniculate nucleus. *J Physiol (Lond)* 496: 759–772, 1996.

PERRAIS D AND ROPERT N. Effect of zolpidem on miniature IPSCs and occupancy of postsynaptic $GABA_A$ receptors in central synapses. *J Neurosci* 19: 578–588, 1999.

QIAN J, COLMERS WF, AND SAGGAU P. Inhibition of synaptic transmission by neuropeptide Y in rat hippocampal area CA1: modulation of presynaptic Ca^{2+} entry. *J Neurosci* 17: 8169–8177, 1997.

SALIN PA AND PRINCE DA. Spontaneous $GABA_A$ receptor-mediated inhibitory currents in adult rat somatosensory cortex. *J Neurophysiol* 75: 1573–1588, 1996.

SOMOGYI P, HODGSON AJ, SMITH AD, NUNZI MG, GORIO A, AND WU JY. Different populations of GABAergic neurons in the visual cortex and hippocampus of cat contain somatostatin- or cholecystokinin-immunoreactive material. *J Neurosci* 4: 2590–2603, 1984.

SOMOGYI P, TAMAS G, LUJAN R, AND BUHL EH. Salient features of synaptic organisation in the cerebral cortex. *Brain Res Rev* 26: 113–135, 1998.

SPRUSTON N, JAFFE DB, AND JOHNSTON D. Dendritic attenuation of synaptic potentials and currents: the role of passive membrane properties. *Trends Neurosci* 17: 161–166, 1994.

STUART GJ AND SAKMANN B. Active propagation of somatic action potentials into neocortical pyramidal cell dendrites. *Nature* 367: 69–72, 1994.

SUN Q-Q, AKK G, HUGUENARD JR, AND PRINCE DA. Differential regulation of GABA release and neuronal excitability mediated by neuropeptide Y_1 and Y_2 receptors in rat thalamic neurons. *J Physiol (Lond)* 531: 81–94, 2001.

TAMAS G, BUHL EH, AND SOMOGYI P. Fast IPSPs elicited via multiple synaptic release sites by different types of GABAergic neurone in the cat visual cortex. *J Physiol (Lond)* 500: 715–738, 1997.

THOMPSON SM AND GÄHWILER BH. Effects of the GABA uptake inhibitor tiagabine on inhibitory synaptic potentials in rat hippocampal slice cultures. *J Neurophysiol* 67: 1698–1701, 1992.

THOMSON AM AND BANNISTER AP. Release-independent depression at pyramidal inputs onto specific cell targets: dual recordings in slices of rat cortex. *J Physiol (Lond)* 519: 57–70, 1999.

THOMSON AM, WEST DC, HAHN J, AND DEUCHARS J. Single axon IPSPs elicited in pyramidal cells by three classes of interneurones in slices of rat neocortex. *J Physiol (Lond)* 496: 81–102, 1996.

TSENG GF, PARADA I, AND PRINCE DA. Double-labelling with rhodamine beads and biocytin: a technique for studying corticospinal and other projection neurons in vitro. *J Neurosci Methods* 37: 121–131, 1991.

ULRICH D AND HUGUENARD JR. $GABA_B$ receptor-mediated responses in GABAergic projection neurones of rat nucleus reticularis thalami in vitro. *J Physiol (Lond)* 493: 845–854, 1996.

VAUTRIN J AND BARKER JL. How can exocytosis account for the actual properties of miniature synaptic signals? *Synapse* 19: 144–149, 1995.

XIANG Z, HUGUENARD JR, AND PRINCE DA. Cholinergic switching within neocortical inhibitory networks. *Science* 281: 985–988, 1998a.

XIANG Z, HUGUENARD JR, AND PRINCE DA. $GABA_A$ receptor-mediated currents in interneurons and pyramidal cells of rat visual cortex. *J Physiol (Lond)* 506:715–730, 1998b.

ZUCKER RS. Short-term synaptic plasticity. *Annu Rev Neurosci* 12: 13–31, 1989.